INTERNATIONAL JOURNAL OF AUTOMOTIVE AND MECHANICAL ENGINEERING
ISSN: 2229-8649 e-ISSN: 2180-1606
VOLUME 23, ISSUE 2, 2026, 13631 - 13648
DOI: https://doi.org/10.15282/ijame.23.2.2026.12.1031

RESEARCH ARTICLE

Optimisation of microscopic defects of wire electrical discharge machining using analysis of variance response optimiser

Rifky Maulana Yusron[1]*, Yuli Panca Asmara[2], Ananto Yusuf Wicaksono[3], Muhammad Azmi Alamsyah[4]

[1]Department of Mechanical Engineering, Universitas Trunodjoyo Madura, Bangkalan, East Java 68162, Indonesia
[2]Department of Mechanical Engineering, INTI International University, Negeri Sembilan 71800, Malaysia
[3]Department Mechanical and Industrial Engineering, Warsaw University of Life Sciences, 166-02-787 Warsaw, Poland
[4]Department of Industrial Management, National Taiwan University of Science and Technology, 106335 Taipei, Taiwan

Abstract - Wire Electrical Discharge Machining (WEDM) employs the principle of electro-thermal discharge, utilising an electric current applied to a wire to generate heat. The process entails liquefying the workpiece material, then vaporising it, and expelling the vaporised material with a dielectric fluid. The research investigates the microscopic characteristics and surface integrity resulting from WEDM of heat-treated high-carbon alloy steel, providing critical insights for precision manufacturing applications. Buderus 2080 high-carbon steel, heat-treated to a hardness of 801 VHN, was machined using WEDM. This research systematically varied pulse-on time (0.2, 0.4, 0.6 µs) and open voltage (75, 90, 105 V) as independent parameters. Surface roughness, recast layer thickness, recast layer hardness and crater width were evaluated as dependent variables. A General Linear Model Factorial as experimental design and Analysis of Variance (ANOVA) were utilised to ascertain the contribution of each independent variable. The findings indicate a direct proportional relationship between pulse-on time and open voltage on the one hand and surface roughness, recast layer thickness and crater width on the other hand. Conversely, a reciprocal proportionality is observed between pulse-on time and the recast layer hardness. Pulse-on time exerted a stronger influence on all dependent variables than open voltage. Optimal machining conditions, determined using the Variance response optimiser, were a pulse-on time of 0.4µs and an open voltage of 90V.

Article History
Received : 14 June 2025
Revised : 16 November 2025
Accepted : 10 December 2025
Published : 30 June 2026

Keywords
Crater width
Pulse on time
Open voltage
Recast layer
Surface roughness
Wire electrical discharge machining

1. Introduction

Wire Electrical Discharge Machining (WEDM) is an indispensable manufacturing process in industries that require high precision. WEDM with two-axis motion can machine complex geometries in high-hardness materials [1]. The material removal mechanism in WEDM is localised melting and vaporisation of the workpiece. This is done by controlled electrical discharges between the continuously fed wire electrode and the workpiece. After that, the workpiece is flushed by a dielectric fluid [2]. There are several strategies used to meet the high-precision requirements of modern manufacturing industries, especially to optimise WEDM process parameters [3]-[4]. The selection and adjustment of parameters have been shown to directly affect the machining efficiency, surface finish, and dimensional accuracy of the workpiece [5]-[6]. Moreover, maintaining surface quality is very important because it affects not only the precision and the functional features of the manufactured components but also their performance and durability [7]. It is evident that a good surface finish is necessary to decrease friction, increase wear resistance and prevent fatigue failures in critical applications [8]. A systematic study of the relationship between machining parameters and surface quality enables industries to ensure that their production processes consistently produce components within strict specifications and industry standards [9]. Pulse on time (PonT) refers to the time duration during which electrical energy is supplied to the workpiece in each pulse. The process is assisted by a spark discharge between the wire and the workpiece, which melts and vaporises a small amount of material. PonT is a parameter that determines the pulse duration during the cutting process [10]. Open voltage (OV) is the voltage applied across the gap between wire and workpiece prior to a spark discharge. As the voltage reaches a threshold, the gap ionises, and a spark jumps between the wire and the workpiece, initiating material removal. OV is an important parameter controlling the energy of the generated sparks [11]. It is necessary to adjust the PonT and OV variables appropriately to reduce surface roughness (SR) and the recast layer (RL). Substantial research has been dedicated to optimising WEDM parameters for various materials, with a particular focus on performance characteristics such as Material Removal Rate (MRR), SR, kerf width, and wire wear. For example, the study on Inconel 825 revealed that the MRR depends directly on PonT and inversely on pulse-off time (PofT), while the wire tension also affects the MRR [12]. Similar studies conducted on AISI 431 stainless steel showed a positive correlation between SR and PonT, and negative correlations with higher PofT and servo voltage. Moreover, the machined surface hardness increased with increasing PonT [13]. Optimisation results for Aluminium 5454 alloy indicated that taper angle, peak current, and PonT affected kerf width, SR, MRR, and wire wear, and that higher currents could affect SR [14]. The study on polycrystalline silicon carbide showed that the OV and servo voltage directly affect MRR, kerf loss, and SR, with the OV directly affecting the rate of formation [15].

Furthermore, PonT and PofT were identified as highly significant parameters for both SR and MRR in medium carbon steel [16]. However, some studies have shown opposite findings. For instance, the study of A309H stainless steel found

***CORRESPONDING AUTHOR | R. Yusron** | ✉ rifky.myusron@trunojoyo.ac.id

that PofT was the main factor for SR, and voltage dominated MRR, with PonT having a relatively lower influence [17]. These studies provide useful information regarding the individual or combined effects of different WEDM parameters on different materials and performance metrics. There is a significant gap in the comprehensive understanding of the interdependent effects of PonT and OV, particularly regarding microscopic surface characteristics such as SR, RL thickness, and RL hardness in heat-treated high-carbon alloy steel. Many existing works focus mainly on MRR or SR, neglecting a detailed microstructural analysis of the RL properties, especially its hardness, in relation to these key parameters for such a critical engineering material. The aim of this study is to precisely evaluate the combined effect of PonT and OV on the microscopic surface defect SR, RL thickness and RL hardness. The present work aims to elucidate the individual and synergistic contributions of these key parameters through systematic experimental design and statistical analysis. The results will significantly enhance understanding of the effects of WEDM on the microstructural integrity and performance of high-carbon alloy steel parts, providing a strong foundation for improving precision and quality in important manufacturing applications and filling a significant gap in the existing literature on WEDM of advanced materials.

2. Material and Methods

2.1 Material

The material used in this research was Buderus 2080 high carbon alloy steel with an as-received hardness of 610 VHN. The following changes were induced to improve the mechanical properties of the material: an increase in hardness, a reduction in brittleness, homogenisation of the grain structure into austenite and an improvement in wear resistance. These changes were obtained through a complete heat-treatment process of the material. After this treatment, the material had a hardness of 712.60 VHN, which is the maximum hardness specified by the manufacturer. The sequence of heat-treatment steps used in this study is presented in Table 1.

Table 1. Heat treatment process in this research

Step	Heat Treatment Process	Temperature (ºC)	Time (minutes)
1	Soft Annealing	600	60
2	Stress Relieving	600	60
3	Pre-Heating I	600	45
4	Pre-Heating II	960	45
5	Austenitising	960	45
6	Quenching	10	2
7	Tempering I	180	120
8	Tempering II	180	120
9	Tempering III	180	120
10	Carburising	-	45
11	Nitro carburising	-	45

2.2 Specimen Preparation

The cutting process was conducted using a CHMER 32GF WEDM machine. GFMS AC Cut VS900 zinc-coated brass wire electrode with a diameter of 0.25 mm was employed for wire cutting. The cutting scheme for WEDM specimen preparation is illustrated in Figure 1.

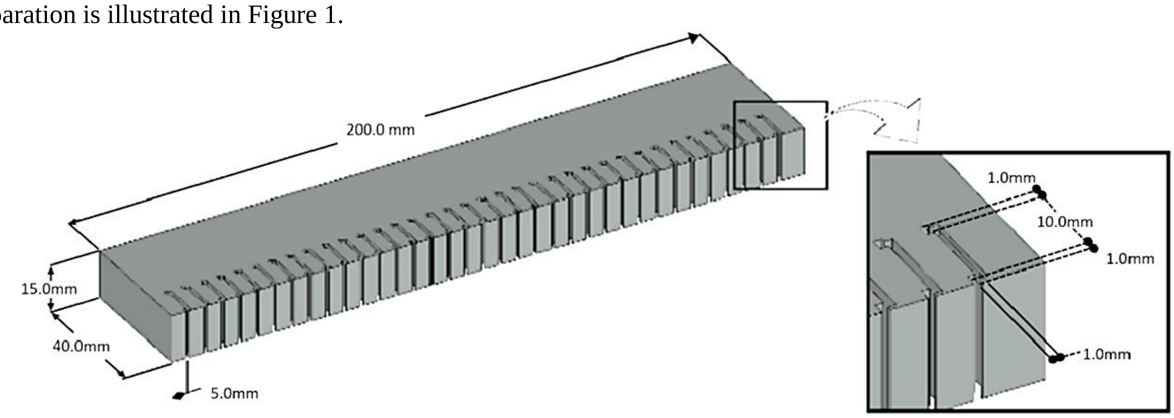

Figure 1. Cutting scheme for this research

2.3 Experimental Design

The experimental design used a 3^2 full factorial design, which systematically investigates the influence of two independent factors, each set at three distinct levels, thereby enabling comprehensive analysis of their individual effects and potential interactions. The independent variables selected for this research were PonT and OV, with their respective levels detailed in Table 2. To ensure the reliability and trustworthiness of the research findings, each combination was replicated three times. This approach, combined with randomisation of the experimental sequence, eliminates potential bias and ensures equal probability [18]. The integration of replication and randomisation has been shown to significantly strengthen the integrity and validity of research and to increase confidence in the obtained results [19]. The constant WEDM process parameters are summarised in Table 3. The machining process was conducted with the workpiece fully submerged in deionised water, which served as the dielectric fluid. All experiments were performed at room temperature (approximately 23 ± 2 °C). The control variables are shown in Table 3.

Table 2. Independent variables in this research

Factor	Level	Value	Unit	Data Type
Pulse on time	3	0.2; 0.4; 0.6	µs	Fix
Open voltage	3	75; 90; 105	V	Fix

Table 3. Control variables of this research

Parameter	Value	unit
Power setting	10	DCEN
Arc of time	13	µs
Pulse-off time	12	µs
Wire feed rate (Override)	9	mm/s
Wire tension	8	G
Wire feed speed	10	mm/s
Dielectric flushing flowrate	6	kg/cm²
Feed rate mode	0	(servo)
Cutting feed rate	1	mm/s
Peak current	2	A
Servo voltage	50	V
Dielectric flushing flowrate	6	kg/cm²

2.4 Measurement of Dependent Variables

The dependent variables investigated in this research were SR, RL thickness, and the recast layer microhardness (RLH). SR measurements were performed using a Mitutoyo Surftest 301 SR apparatus. Measurements were taken perpendicular to the wire-cutting path on the workpiece surface as shown in Figure 2(a). RL Thickness was observed using a Scanning Electron Microscope (SEM) (Inspect S50) with 2000X magnification. The thickness of RL was measured using computer-aided design software. RL measurements were taken three times (right, centre, and left), as depicted in Figure 2(b). Each side was further replicated ten times to ensure statistical robustness. RH was determined using a Vickers microhardness tester, specifically a Wilson 402MDV. The precise locations for microhardness measurements on the specimen and its dimensions are illustrated in Figure 2(c).

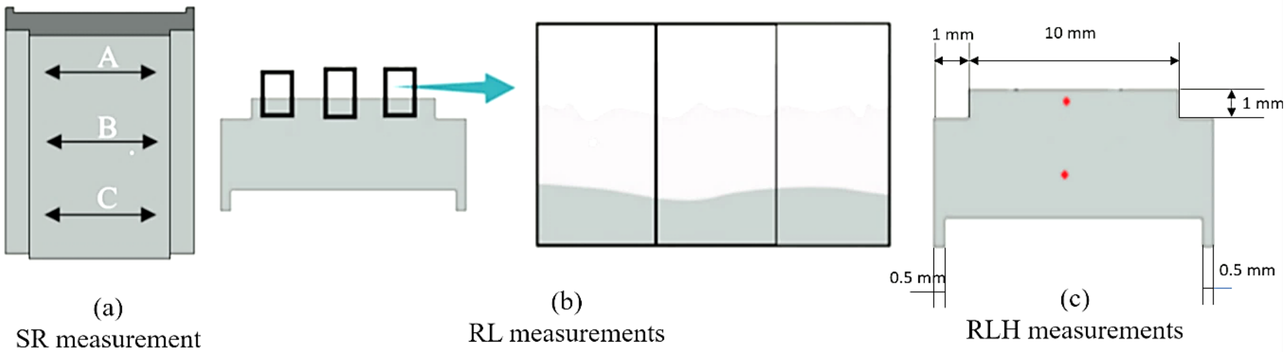

Figure 2. Measurement scheme of dependent variable in this research

3. Results and Discussion

Experiments were conducted to investigate the effects of pulse-on time (PonT) and open voltage (OV) on the WEDM machining process. The experimental results are summarised in Table 4. The lowest SR obtained in this study is 1.33 µm, as shown in Table 4, at PonT 0.2 µs and OV 75V in the first replication. The highest SR value of 2.53 µm was achieved at PonT 0.6 µs and OV 105V. These results show that the surface finish deteriorates significantly as PonT and OV increase. The lowest RL layer thickness reached in this study was 4.34 µm for a machining combination of 0.2 µs PonT and 75V of OV at the third replication. In contrast, the maximum RL thickness of 6.61 µm was achieved at 0.6 µs PonT and 105V OV in the third replication. This trend indicates that higher discharge energy conditions lead to greater material melting and resolidification, resulting in thicker RL formation. The maximum RLH was 698.42VHN at 0.2 µs PonT and 75V OV, whereas the minimum RLH value of 609.03 VHN was observed at 0.6µs PonT and 105V OV in the third replication. The opposite trend indicates that higher thermal input during machining reduces the hardness of the RL due to changes in the resolidified microstructure. In general, the independent variables PonT and OV showed a positive proportional relationship with SR and RL thickness and an inverse proportional relationship with RLH. A similar study [20] reported SR values in the range of 3-4 µm. The higher SR values reported in that study were attributed to the use of Inconel 718, which has a lower hardness of 296 VHN than the material used in the present work. In addition, the PonT used in that study was 300 µs, which contributed to the higher SR. In related work [21] and [22], it has been demonstrated that quenching and controlled heating of heat-treated materials result in finer grain sizes. The SR and the erosion efficiency in WEDM are higher for finer-grained structures, such as those in quenched steels, at the same PonT and OV.

Table 4. Result of the experiment

Run Order	PonT (µs)	OV (V)	SR (µm)	RL (µm)	RLH (VHN)	CW ($µm^2$)
1	0.6	75	2.08	5.62	635.24	753.668
2	0.6	90	2.25	5.97	634.39	861.712
3	0.2	105	1.65	5.14	647.00	543.111
4	0.4	105	2.04	5.54	639.99	571.269
5	0.4	105	2.14	5.44	633.59	581.644
6	0.6	90	2.25	5.83	618.90	861.712
7	0.6	90	2.15	5.80	627.80	821.423
8	0.2	90	1.48	4.55	669.80	345.858
9	0.2	75	1.33	4.53	698.42	389.264
10	0.2	75	1.39	4.38	680.70	449.220
11	0.2	75	1.42	4.44	689.90	420.411
12	0.2	105	1.65	5.09	648.77	566.187
13	0.6	105	2.52	6.14	611.47	905.834
14	0.6	75	2.08	5.69	632.25	801.144
15	0.6	105	2.52	6.16	614.92	954.500
16	0.4	75	1.69	5.28	656.82	580.788
17	0.4	75	1.78	5.10	652.33	566.298
18	0.4	90	1.87	5.44	650.88	549.067
19	0.6	105	2.53	6.61	609.03	887.445
20	0.4	90	1.77	5.33	648.77	602.657
21	0.4	90	1.80	5.54	645.24	579.522
22	0.4	75	1.71	4.93	654.72	566.298
23	0.2	105	1.70	4.88	650.12	588.087
24	0.6	75	2.20	5.76	634.80	782.222
25	0.4	105	2.20	5.53	639.80	621.947
26	0.2	90	1.58	4.77	670.11	380.858
27	0.2	90	1.60	4.99	668.71	377.252

3.1 Surface Roughness Response Analysis

SR is an essential characteristic for surface identification and for evaluating materials that have undergone machining processes [23]. SR and PonT are directly proportional, as mentioned in Table 3. High PonT values promote "double sparkling," in which increased pulse duration leads to a higher frequency of electrical sparks [24]. This results in increased thermal energy delivered to the workpiece, thereby enhancing heat conduction, increasing erosion, and forming deeper craters, which consequently elevate SR. Similarly, an elevated OV intensifies the electric field between the workpiece and the electrode, leading to more stable and efficient sparks and, consequently, greater material erosion. The augmented discharge energy associated with elevated OV generates additional heat, further impacting SR. A previous study on heat-treated steel has also reported that insufficient flushing during machining increases SR. The double-sparking phenomenon was evident at PonT values of 0.4 µs and 0.6 µs. Enhancing OV increases the potential difference between the workpiece and the electrode wire. Consequently, the electric field intensifies, leading to increased stability and efficiency of the sparks within the same gap. This results in a greater volume of eroded material, which directly influences the measured SR on the workpiece surface. Consistent findings have been reported [25] in heat-treated steel and in cold work, where SR increases when the workpiece is not adequately flushed during machining. The results of statistical tests using the general linear model (GLM) ANOVA are shown in Table 5. Table 5 demonstrates how the variables PonT and OV influence SR. It presents the results of the GLM ANOVA, showing that both PonT and OV have a statistically significant impact on SR, with p-values of 0.000 for both factors. Table 5 shows the effects of the variables PonT and OV on SR. Results of the GLM ANOVA are shown, with both PonT and OV having statistically significant effects on SR ($p< 0.001$ for both factors). PonT is the main factor of SR variation with 78.33% contribution, and OV contributes 18.86%. Note that a full-factorial experimental design was used, which generally facilitates the analysis of interaction effects, but the ANOVA table below does not explicitly report the contribution or statistical significance of the PonT-OV interaction term. When interpreting the individual effects of PonT and OV on SR, this limitation has to be considered. In WEDM processes, parameters do not work independently, and their coupled effects can influence surface characteristics [26]. Thus, although the individual contributions of PonT and OV are relevant, a better understanding can be achieved by incorporating interaction analysis, as reported in previous studies on materials such as AISI 304 stainless steel and Inconel 718 [27], [28].

Table 5. Results of GLM ANOVA on SR variable response

Source	DF	Seq SS	Contribution	F-Value	P-Value
PonT	2	2.54881	78.33%	305.88	<0.001
OV	2	0.61365	18.86%	73.64	<0.010
Error	22	0.09166	2.82%		
Lack-of-Fit	4	0.03846	1.18%	3.25	0.036
Pure Error	18	0.05320	1.63%		
Total	26	3.25412	100.00%		

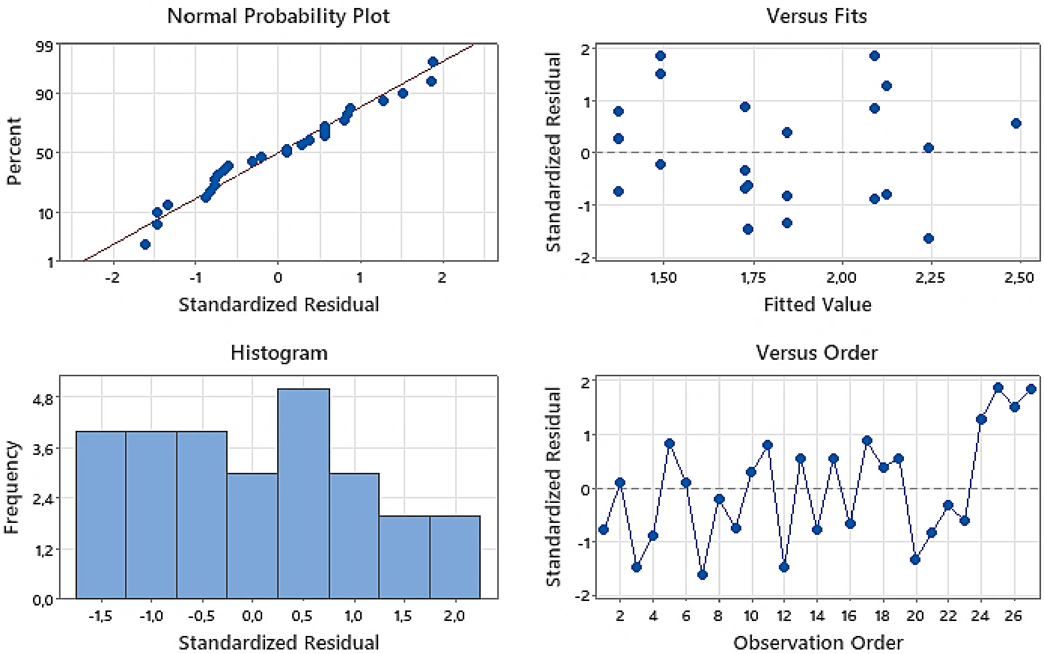

Figure 3. Result of residual plot on SR variable response

Figure 3 shows that the residual plots validate the statistical model's assumptions. The Normal Probability Plot and Histogram confirm the approximate normal distribution of residuals. The Versus Fits plot shows a random scatter around the zero line, indicating constant variance (homoscedasticity) and linearity. The Versus Order plot reveals a random distribution, confirming residual independence. Collectively, these diagnostic plots confirm that the model's assumptions are adequately met, thereby ensuring the reliability and validity of the ANOVA results regarding the influence of PonT and OV on SR.

3.2 RL Response Analysis

During the PonT phase, the cutting process occurs. During the Toff phase, cutting does not occur [29]- [30]. This phenomenon occurs on a microsecond timescale and repeats continuously, leading to rapid cooling via the dielectric fluid. When the workpiece is flushed with dielectric fluid, the eroded material detaches from it. Material erosion is the mechanism by which the cutting process takes place in WEDM [31]. The PonT determines the frequency of the cutting phase, whereas OV determines the magnitude of the cutting energy. An elevated level of the PonT factor leads to a higher frequency of sparks colliding with the workpiece, thereby causing the material to undergo progressively greater melting and solidification [32]. Increasing OV will result in a greater transfer of thermal energy to the workpiece, leading to a greater distance over which heat conducts from the workpiece's surface. As the values of PonT and OV increase, erosion of the workpiece material intensifies, leading to thicker recast layers.

Some recast layers (RLs) observed in this investigation showed a tendency to contour. Figures 4(C-F) demonstrate that certain RL surfaces exhibit a propensity for being curved, while Figure 4(A and B) displays a tendency for being flat. When the PonT factor is modest and the OV factor is significant, the resulting RL tends to exhibit a more uniform and flatter morphology. This phenomenon occurs because sparks occur infrequently, resulting in reduced erosion of the workpiece surface. Consequently, the RL exhibits a predominantly flat shape. Conversely, when the PonT factor was high and OV was low, the RL tended to exhibit a contoured morphology. Increased PonT intensifies the frequency of thermal energy transfer to the workpiece. As the discharge energy increases, the volume of molten material also increases, leading to uneven solidification and distinct surface contours within the RL. Elevated OV further increased heat conduction, promoting deeper erosion of the workpiece and a greater accumulation of molten and resolidified material. As a result, the difference in RL contour becomes more pronounced when the PonT and OV settings are set at high levels. Figure 4(A) presents the RL formed from the combination of PonT 0.2 µs and OV 75 V, which exhibited a predominantly flat morphology with a relatively uniform thickness. The RL formed by this combination tends to be uniform, ranging from approximately 3.16 µm to 4.48 µm, with an average value of 4.53 µm. Figure 4(B) is an image of the RL formed in the combination of PonT 0.2µs and OV 90V machining process. The RL formed is nearly the same as the combination in Figure 4(A), but the RL value spans a wider thickness range of 3.51-5.1 µm, with an average thickness of 4.99 µm, higher than that in Figure 4(A). Figure 4(C) shows that the RL exhibits a flat trend and a uniform thickness. The mean thickness of the RL is 5.12 µm. Figure 4(D) illustrates that the RL formed tends to be contoured, resulting in a distinctly non-uniform thickness. The thickness ranges from 3.28 µm to 8.78 µm, with an average thickness of 5.39 µm. As illustrated in Figure 4(E and F), the RL formed tends to be contoured, resulting in a non-uniform thickness. The mean layer thickness is 5.28 µm. Figure 4(F) displays a contoured RL formation similar to that observed in Figure 4(C), albeit with some regions exhibiting thinner RL and others displaying thicker RL. In this configuration, the minimum RL thickness is 3.43 µm, while the maximum R thickness is 9.49 µm. The RL thickness exhibits a non-uniform distribution, falling within a broader range. The mean RL thickness was 5.89 µm. According to the reported study [33], non-uniform RL formation was achieved using a different EDM sinking machining and a titanium composite material.

Table 6. Result of GLM ANOVA on RL variable response

Source	DF	Seq SS	Contribution	F-Value	P-Value
PonT	2	6.4922	78.34%	138.96	0.000
OV	2	1.2806	15.45%	27.41	0.003
Error	22	0.5139	6.20%		
Lack-of-Fit	4	0.1107	1.34%	1.24	0.331
Pure Error	18	0.4032	4.87%		
Total	26	8.2867	100.00%		

Table 6 shows the GLM ANOVA results, which clearly indicate that PonT and OV have statistically significant effects on RL thickness, with P-values of 0.000 and 0.003, respectively. The largest contribution is made by PonT, which accounts for 78.34% of the total variation, while OV accounts for 15.45%. Although a full factorial experimental design was adopted, the ANOVA results did not explicitly report the PonT-OV interaction. This limitation should be kept in mind when interpreting the individual effects of these parameters on RL formation. In WEDM processes, electrical parameters can be correlated and influence surface integrity characteristics, such as RL thickness [34]. For example, the optimum PonT level for reducing or controlling RL thickness may vary for a given OV setting. Many studies have highlighted the importance of accounting for interaction effects in modelling and optimisation of WEDM processes. Another study revealed significant interactions between PonT and other parameters and surface integrity, including RL formation, across different materials [35]. Similarly, earlier studies have reported that the interactions between electrical parameters significantly affect the RL characteristics of advanced alloys [36]. Ignoring these interactions may lead to a poor understanding of the complex thermal and metallurgical phenomena occurring during the WEDM process, resulting in suboptimal process control and incorrect conclusions about the effects of process parameters [37]. So, although the effect of PonT is dominant, the addition of interaction terms would give a better insight into the mechanisms that control the formation of RL. The RL formation observed in this research at the combination parameter of 0.2 µs for PonT and 75 V for OV 4(A) is shown in Figure 4. RL formation at the combination parameter of 0.2 µs of PonT and 90 V of OV 4 (B). RL formation at the combination parameter of 0.2 µs of PonT. 105 V of OV 4(C). 0.4 µs of PonT and 105 V of OV 4(D) 0.6 µs of PonT and 90 V of OV 4(E) on combination 0.6 µm RL formed. PonT of 0.6 µs and OV of 105 V (F).

Figure 5 shows the observed RL thickness in this observation, ranging from 7.88 µm to 35.33 µm, with an average of 22.583 µm, indicating a significant thermal impact on the heat-treated Buderus 2080 during the WEDM process. thickness of this range is significantly larger than the reported RL of 2.53 µm for a heat-treated specimen under similar machining conditions. The high temperature during electrical discharges results in localised melting and subsequent rapid solidification of the workpiece material, directly consequent on the formation of the RL. The large thickness achieved in the present study can be attributed to the specific combination of high energy input parameters, particularly the different PonT and OV. Similar studies on AISI M2 steel with a high carbon content have confirmed the hypothesis that longer pulse durations result in thicker RL. This is explained by an increase in the volume of molten material as energy input per pulse increases [38]. Similarly, studies on different alloys, such as Inconel 718, highlight the importance of high discharge energy. Parameters such as PonT often dictate the extent of melting, resulting in increased melting and, hence, a more pronounced RL [39]. Furthermore, material properties such as thermal conductivity, melting point, and the specific heat treatment used to achieve a hardness of 801 VHN are of utmost importance for determining the degree of melting and re-solidification [40]. The presence of a thick RL underscores the importance of electrical discharge parameters and the characteristics of the heat-treated high-carbon alloy steel in determining the resulting surface integrity.

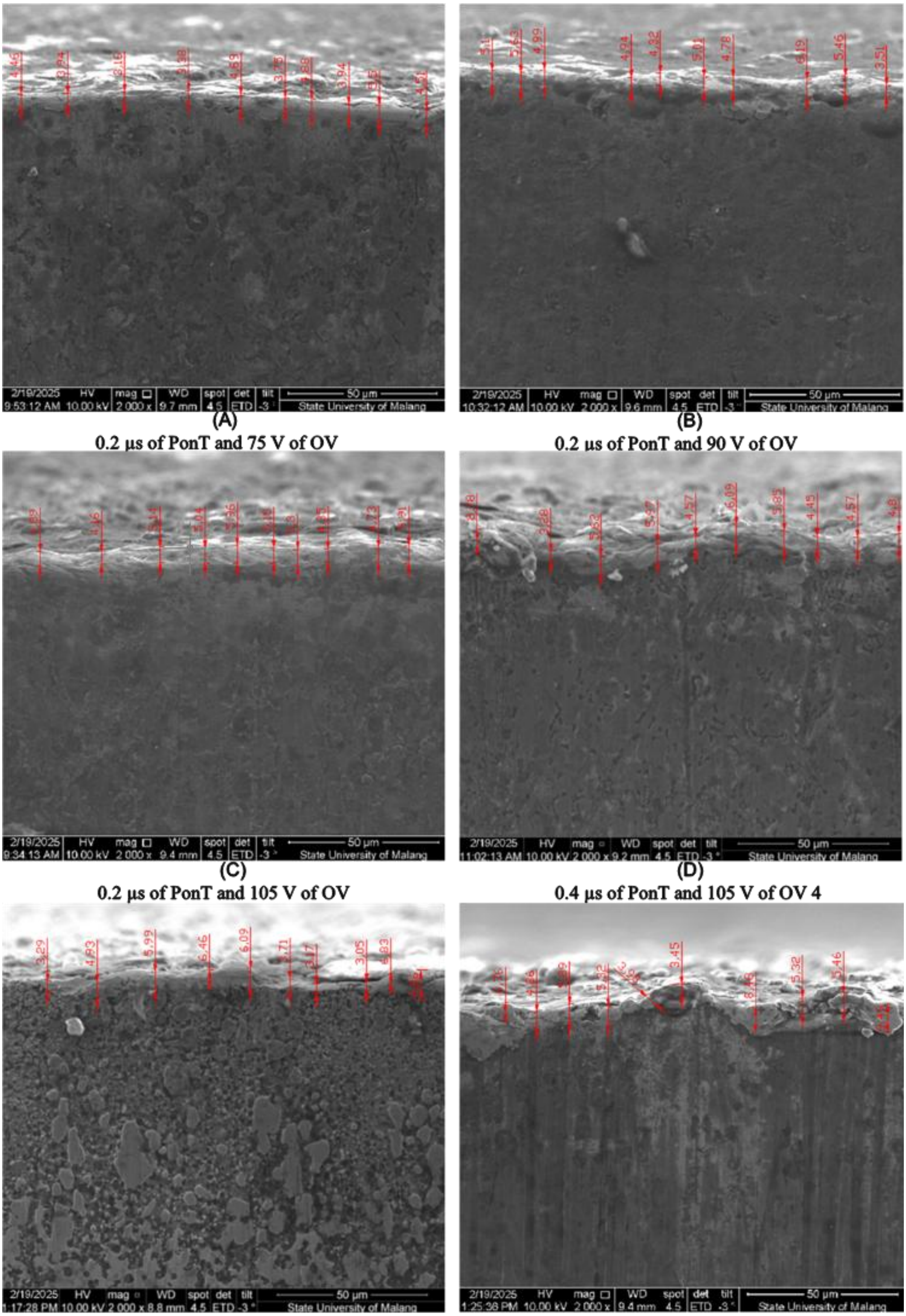

(A) 0.2 µs of PonT and 75 V of OV

(B) 0.2 µs of PonT and 90 V of OV

(C) 0.2 µs of PonT and 105 V of OV

(D) 0.4 µs of PonT and 105 V of OV 4

(E) 0.6 µs of PonT and 90 V of OV

(F) 0.6 µs of PonT and 105 V of OV

Figure 4. RL formed by heat-treated specimen in this research resulted by each machining parameter

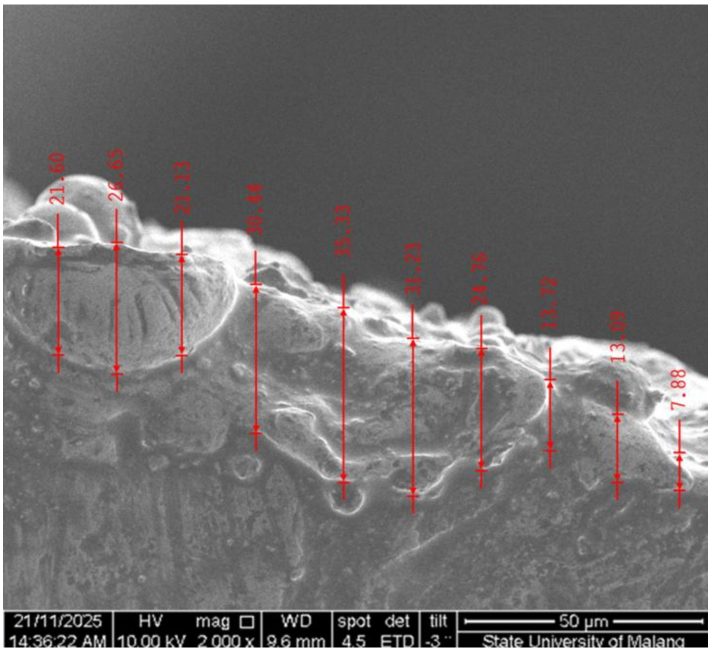

Figure 5. RL formed by non-heat-treated specimen using 0.6 µs of PonT and 105V of OV

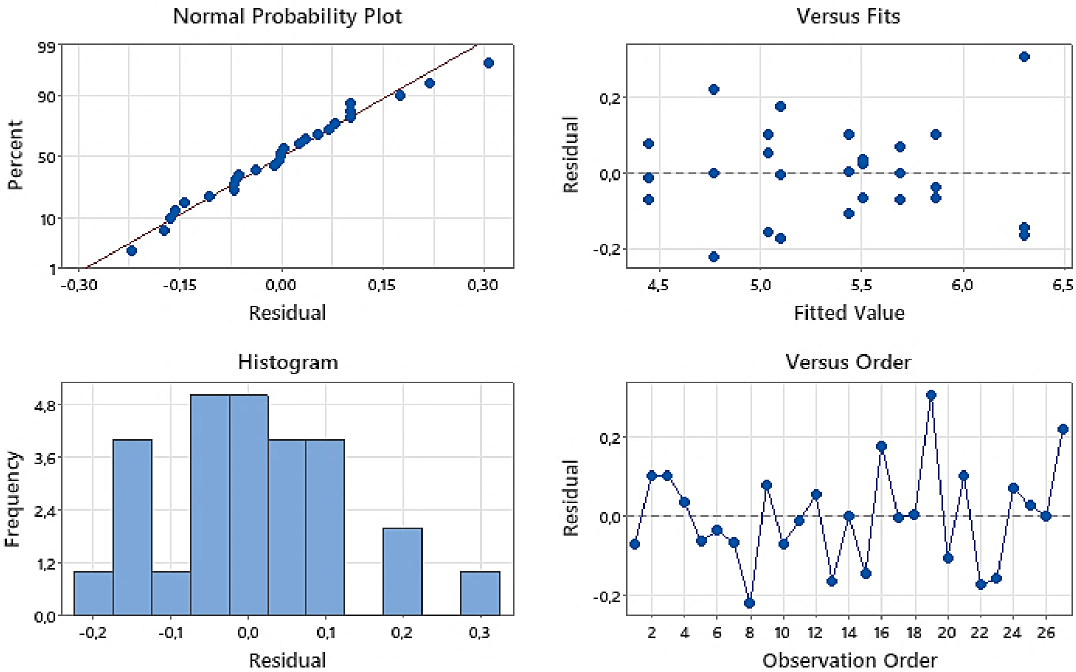

Figure 6. Result of residual plot for RL response

Figure 6 shows that the residual plots support the statistical model's assumptions for the RL data. The Normal Probability Plot and Histogram confirm normality. The Residual versus Fits plot shows a random scatter, fulfilling the assumption of homogeneity of variance. The Residual versus Order plot confirms the residuals are independent. These collectively ensure the reliability of the RL experiment.

3.3 Recast Layer Hardness Response Analysis

According to the microhardness data presented in Table 3, microhardness decreases within the RL. The reduction in microhardness in the RL is due to the workpiece undergoing a prior heat treatment before WEDM. The purpose of heat treatment is to attain the material's greatest achievable hardness. The WEDM technique employs thermal energy to penetrate the workpiece. The temperature applied to the workpiece can range from 8,000 °C to 20,000 °C, as reported by [41]. Causing the workpiece to melt. The rapid melting and solidification of the workpiece do not occur uniformly throughout the workpiece but only on the surface subjected to the cutting process. This specific region is referred to as the RL [42]. Increasing PonT increases the frequency of sparks, leading to greater melting and solidification of the workpiece material. OV intensifies the electric field, increasing heat conduction and distributing thermal energy more evenly throughout the workpiece. Repeated intense thermal impacts increase heat absorption, reducing the cooling rate and slowing the solidification process. Conversely, minimal heating promotes rapid cooling and faster solidification. This rapid solidification process, characteristic of WEDM, can trap air and form voids within the RL, thereby decreasing its microhardness. This inverse relationship between PonT or OV and RLH aligns with the findings of other studies. Microhardness indentation analysis (Figure 7) shows that all indenters successfully penetrated the RL and reached the parent material, despite the varying thicknesses of the RL (Table 3). For example, with the lowest PonT (0.4 µs) and OV (90 V), the RL thickness was 4.53 µm, and the indentation depth was 7.83 µm. This resulted in a high microhardness of 698.42 VHN, indicating a significant influence from the parent material. In contrast, a combination of high PonT and OV yielded an RL thickness of 6.16µm and an indentation depth of 8.39µm. This suggests that, although thicker RLs offer greater initial resistance to indentation, measured hardness values are significantly influenced by the underlying parent material, especially when the indentation depth exceeds the RL thickness. A similar phenomenon was observed in a study by Chakraborty et al. [43].

Table 7. Result of GLM ANOVA on RLH variable response

Source	DF	Seq SS	Contribution	F-Value	P-Value
PonT	2	9100.4	68.95%	116.80	<0.001
OV	2	3241.7	24.56%	41.61	<0.001
Error	22	857.0	6.49%		
Lack-of-Fit	4	497.5	3.77%	6.23	0.03
Pure Error	18	359.5	2.72%		
Total	26	13199.2	100.00%		

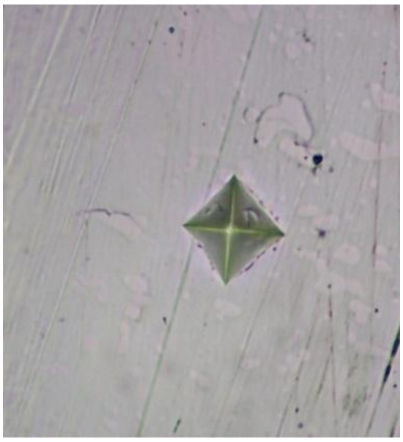

Figure 7. The indenter results during measurement in this research and the indenter shape

The GLM ANOVA results for the RLH response variable are shown in Table 7 and indicate that both PonT and OV had a statistically significant effect on this key surface property (p-values < 0.001). PonT is the dominant factor, explaining 68.95% of the variation in RLH, followed by OV at h 24.56%. Although the experimental design was full factorial, which allows investigation of interaction effects, the ANOVA table reported only the main effects of PonT and OV. The absence of an explicit interaction term between PonT and OV in the presented results restricts a complete understanding of how these two electrical discharge parameters might affect RL hardness synergistically or antagonistically. The complex interplay among process parameters in WEDM often implies that their combined effects are not simply additive; rather, they can exhibit significant interactions that profoundly influence the resultant surface integrity, including RLH [44]. Hardness of the RL is an important indicator of its metallurgical structure, which is highly sensitive to the thermal history imposed by the electrical discharges. For example, the optimal PonT setting to obtain a given RLH may depend on the OV level used, and vice versa. If we ignore these interaction effects, we may get an incomplete or even misleading picture of the process mechanics, and we may not be able to precisely control the machined surface properties. The importance of interaction effects has been stressed in the WEDM literature, with many studies emphasising the need to study the complex relationships between the input parameters and output responses. The interaction of PonT with other electrical parameters can significantly influence the microhardness and metallurgical properties of the RL, as observed in studies on various materials, since these interactions govern the localised energy density and cooling rates [45]. While the contributions of PonT and OV to the RLH are certainly important, a detailed study of their interaction would be very useful in optimising the WEDM process to control the mechanical properties of the RL in heat-treated high-carbon alloy steel.

Figure 8 shows that the residual plots validate the GLM ANOVA results for RLH. The Normal Probability Plot and Histogram confirm the normality of the residuals. The Versus Fits plot displays a random scatter, indicating homoscedasticity and adequate model linearity. The Versus Order plot further demonstrates the independence of the residuals. The collective affirmation of these diagnostic plots confirms that the underlying statistical assumptions are satisfied, thereby reinforcing confidence in the ANOVA results presented in Table 7. These findings indicate that PonT and OV significantly influence RLH, with PonT playing a predominant role. This approach ensures the reliability of conclusions regarding their main effects. The robustness of the model, as supported by these residual analyses, ensures that the conclusions drawn regarding the main effects of PonT and OV on RLH are reliable. The indenter results during measurement in this research and the indenter shape are shown in Figure 7.

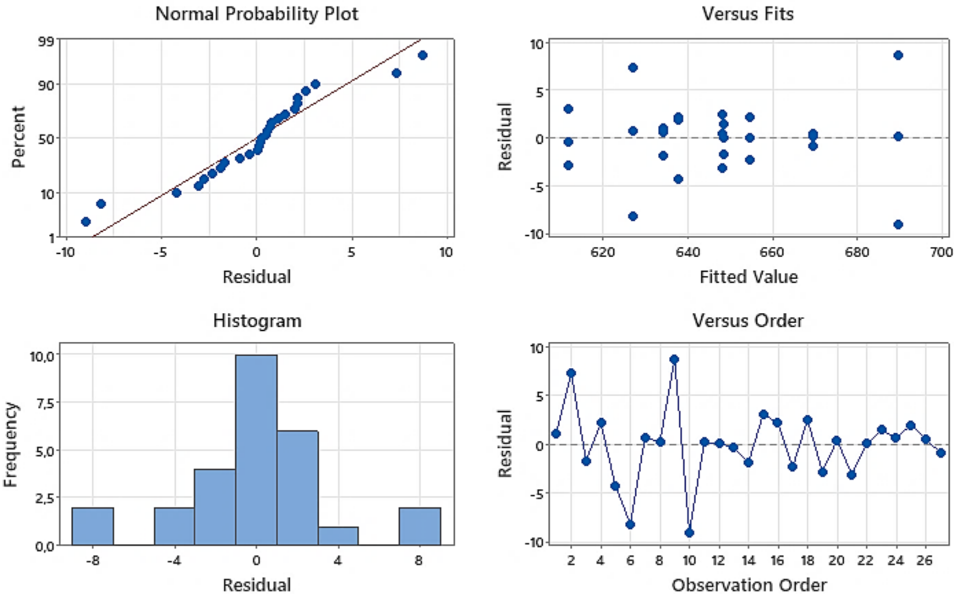

Figure 8. Result of residual plot for RLH response

3.4 Crater Width Response Analysis

The results of WEDM cutting are a series of contoured surfaces. Through topographic observation, various surface-forming phenomena are observed, including, but not limited to, globules, pockmarks and craters. Craters are a major feature of the molten metal and are randomly distributed across the workpiece's surface. The formation of the deposit is attributed to the release of gases from the redeposited material, which subsequently becomes entrapped by the rapidly solidifying material [46]. Pockmarks are formed by material removal during machining, leaving depressions on the workpiece surface. It has been established that a potential difference develops between the electrode wire and the workpiece during machining, leading to localised explosion. The detonation of the explosive material erodes the workpiece, forming craters on its surface. Debris is a component of the workpiece that is removed by erosion during the machining process. As demonstrated in Figures 10(A-B), the surface topography of the heat-treated specimen is presented, while Figure 9(C) presents the surface topography of the specimen that was not subjected to heat treatment.

Figure 9(A) shows the results of surface topography observation using SEM at 2000x magnification on the specimen machined with a 0.2 µs PonT and 75 V OV combination. The distribution of craters is non-uniform and uneven across the entire surface of the workpiece produced by the WEDM process. The crater area varied according to the measurements obtained with ImageJ. The narrowest crater had an area of 2.598 µm², while the largest had an area of 72.125 µm². The overall crater area for this combination was 449.220 µm². It was observed that narrow crater formations tend to occur near larger craters during the PonT phase. This phenomenon can be attributed to the fact that the energy released during machining to erode the workpiece is exclusively during the PonT phase. This energy is sufficiently potent to erode the workpiece. Subsequently, the energy released during the PofT phase allows residual electrical energy to erode the workpiece. However, this energy is insufficient to initiate the cutting process, resulting in a small crater. This phenomenon explains why small craters are frequently found near larger craters. Relevant research Paswan et al [47] revealed that at elevated wire feed and cutting speeds, the resulting crater size is reduced. Another study found that discharge energy is a determining factor in pockmark formation [48].

It has been observed that as the energy increases, the diameter of the pockmark on the workpiece also increases. As illustrated in Figure 9(A), the pockmarks and globules produced in this combination are relatively small. No debris was observed on the workpiece surface during cutting with this combination, although these features were not quantitatively measured in this research. Observations in Figure 9(B) also show that the craters formed by this machining combination are fewer in number, but the craters are also wider. The narrowest crater produced in this combination is 9.105 µm², while the widest is 285.829 µm². The total number of craters in this machining combination is 954.500 µm². The phenomenon of large craters is attributed to the 0.6 µs PonT value used in this combination. As a result, sparks impact the workpiece more frequently, leading to increased erosion. Furthermore, a higher OV value increases the discharge energy during machining, resulting in deeper metal penetration and, consequently, larger crater sizes than pockmarks produced under lower OV conditions. From the surface topography shown in Figures 10(A-B), it can be concluded that PonT is a key factor in determining crater size, whereas OV primarily affects the number of craters. The formation of craters is characterised by a tendency for large craters to be near one another, as well as for narrow craters to be formed. This indicates that large craters form due to high discharge energy during high PonT duration. In contrast, narrow craters are caused during PofT. Further detailed analysis of these variables is required. However, this research indicates that the PofT variable has no significant impact on SR [49]. Additionally, debris was observed on the workpiece surface. The number of globules, pockmarks, and debris affecting the workpiece's surface topographies is presented in the following study [50]. However, globules, pockmarks, and debris were not observed in this research. Figure 9(C) displays the surface topography of the non-heat-treated specimen processed with PonT at 0.6 µs and OV 105 V. The observed crater area was 976.21 μm^2, substantially larger than that for the heat-treated specimen under identical machining conditions. The surface topography consisted of the largest crater area of 868.47 μm^2 and the smallest crater area of 29.82 μm^2. The positions of individual craters were closely spaced, in contrast to the heat-treated specimens, which exhibited numerous pockmarks with diameters ranging from 0.1 to 0.2 μm^2 distributed across the surface. This difference is attributed to the heat treatment processes applied to Buderus 2080 high-carbon alloy steel, particularly carburising and tempering, which are intended to enhance surface hardness and wear resistance [51]-[52]. Reported by Gugulothu et al. [53] contained more cavities, globules, debris, crater on the AISI 304 stainless steel's surface through machining combination PonT 120µs, PofT 50µs, and peak current 16A. Carburising introduces additional carbon into the surface layer, which upon quenching transforms into a dense, wear-resistant martensitic structure. Subsequent tempering relieves internal stresses while maintaining elevated hardness [54]-[55].

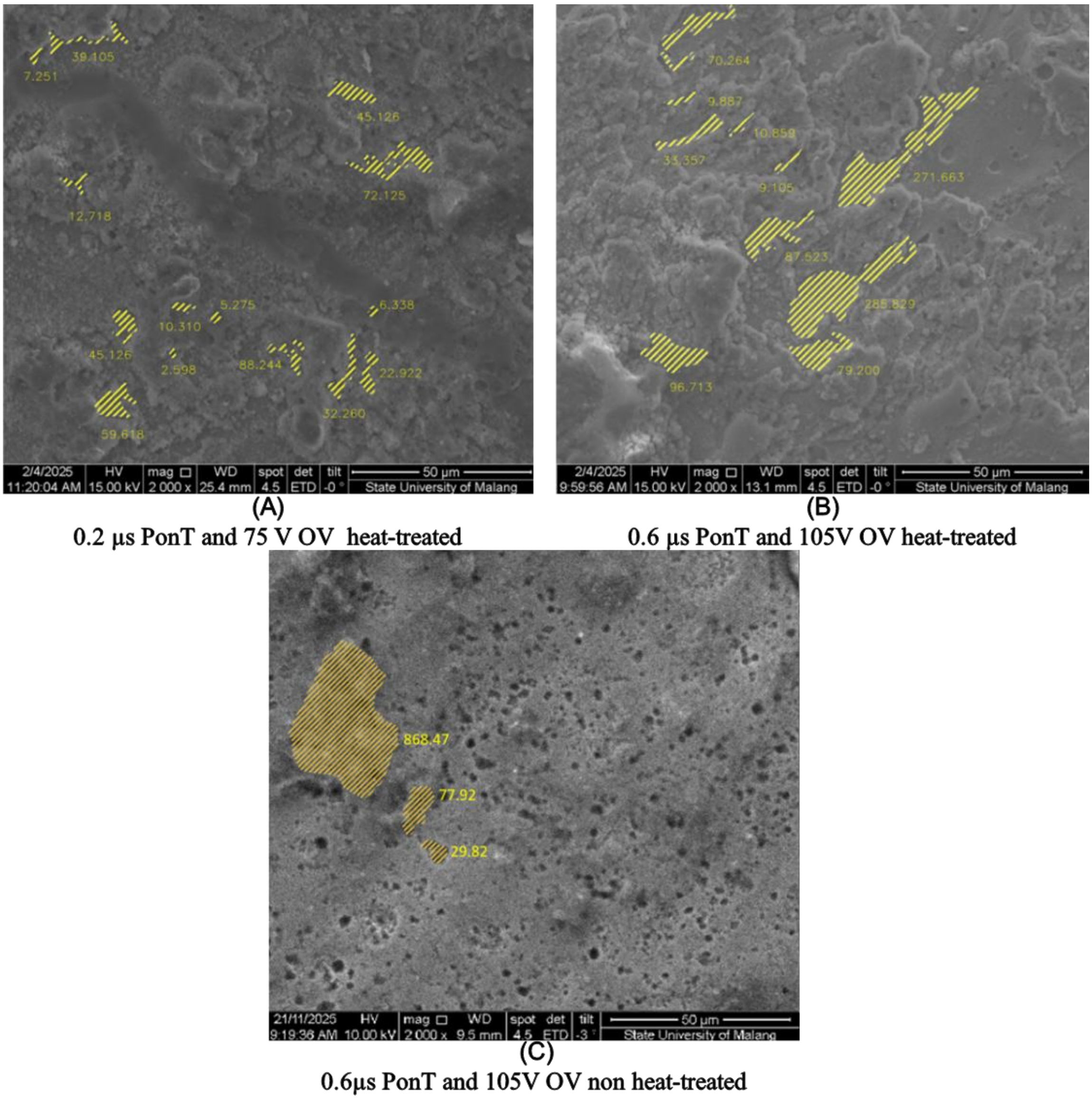

Figure 9. Result of surface topography specimen in this research

As a result, the heat-treated material becomes harder and less ductile, making it more susceptible to brittle fracture during WEDM. WEDM discharges impose severe thermal shocks on the workpiece surface due to rapid localised heating and cooling [56]. In materials with reduced ductility and increased brittleness, these thermal shocks may induce microcracks and material expulsion via brittle fracture mechanisms rather than elastic deformation [57]. The pockmarks observed on the machined surface indicate that brittle material was removed. When localised thermal stress causes materials to spall off, they leave behind uneven depressions. This phenomenon is consistent with observations for other rigid and brittle materials processed by WEDM, in which surface imperfections such as pockmarks and craters are more pronounced due to the material's limited elastic deformation under thermal stress [58]. The observation of surface morphology, including pockmarks, craters, and globules, on the machined surface of heat-treated Buderus 2080 high-carbon alloy steel is a direct consequence of the WEDM process. The specimen is harder and less ductile than it would be if annealed. However, the basic thermal-erosion process in WEDM naturally creates these surface irregularities. The strong, localised electrical discharges quickly melt and vaporise the workpiece material, then cause explosive ejection, followed by rapid solidification of the molten surface. This process, which is subject to constant change, ultimately leads to the formation of craters and depressions that resemble pockmarks on the surface. Research on materials known for their ductility, such as Inconel 718, Ti6Al4V, and AISI 304 stainless steel, has consistently revealed craters, globules, and other surface irregularities after WEDM machining [59]-[61]. For example, the Ti_6Al_4V alloy, known for its high elongation to failure of 15–20% [62], still shows clear craters and globules after WEDM due to thermal shock and material expulsion. AISI 304 stainless steel, which is also very ductile and can stretch by more than 50% [63]-[64], exhibits craters and micro-voids on its WEDM-machined surfaces [65]. Confirmed by Šimna et al. [66], on ductile material leads to higher wire electrode wear, besides machining parameters of 0.8µs of PonT, 16µs of PofT, and 40V of SV. This combination of parameters not only results in the formation of wide craters but also leads to high titanium release from the Inconel 718 alloy. Therefore, if naturally very ductile materials exhibit these flaws, it is even more likely that a heat-treated, high-carbon alloy steel will show clear pockmarks and craters. These characteristics are indicative of localised brittle fracture and material ejection resulting from the extreme thermal gradients and pressure waves produced during the WEDM process.

Table 8. Result of GLM ANOVA on the CW variable response

Source	DF	Seq SS	Contribution	F-Value	P-Value
PonT	2	6.4922	78.34%	138.96	<0.001 (Significance)
OV	2	1.2806	15.45%	27.41	0.003
Error	22	0.5139	6.20%		
Lack-of-Fit	4	0.1107	1.34%	1.24	0.331 (Insignificance)
Pure Error	18	0.4032	4.87%		
Total	26	8.2867	100.00%		

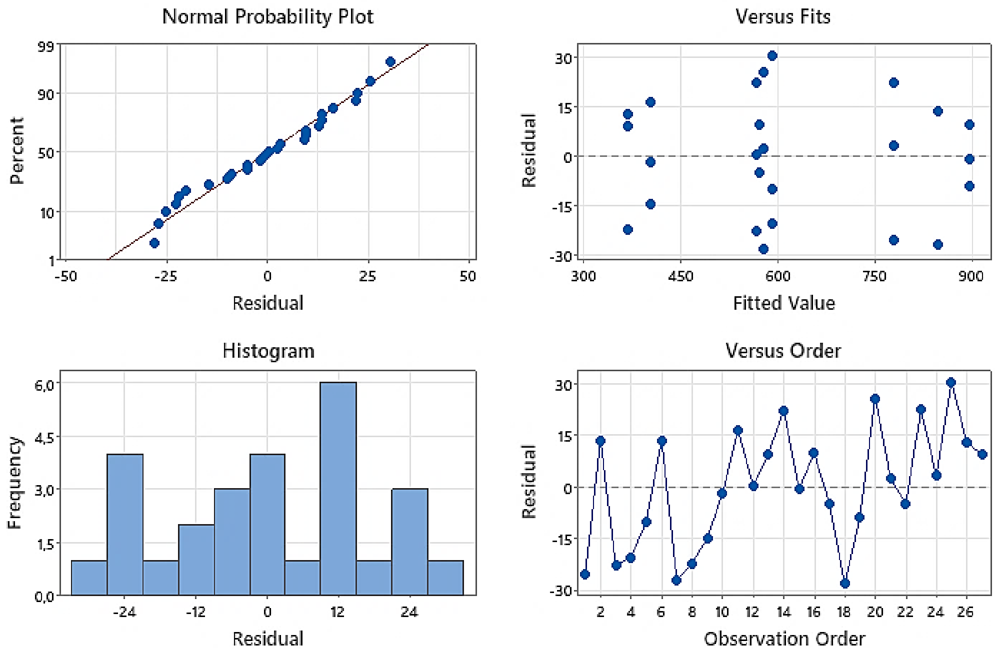

Figure 10. Result of residual plot for CW response

Table 8 shows that both PonT and OV significantly influence CW, with a p-value of 0.000. PonT is identified as the dominant factor, contributing 68.95%, while OV contributes 24.56%. Although a full-factorial experimental design was employed, the ANOVA results focused on the main effects of PonT and OV. Interpretation of CW behaviour should therefore account for the possibility of coupled parameter effects. Crater formation is a direct consequence of localised thermal energy input, which melts and vaporises material. The size and morphology of these craters are highly sensitive to the combined energy delivered by each discharge, which is a function of both the duration of PonT and the potential difference across the gap (OV) [67]. Therefore, the interaction between PonT and OV is particularly crucial for understanding and controlling crater width, as the effect of increasing PonT on CW might either be amplified or mitigated depending on the specific OV setting, and vice versa. Numerous studies in WEDM literature emphasise the importance of analysing interaction effects to fully capture the intricate relationships between input parameters and output responses, especially for surface characteristics. For instance, research on various materials has demonstrated that the interaction between PonT and other electrical parameters can significantly influence surface morphology, including crater dimensions and distribution [68]. The application of a dielectric fluid mixed with 10µm boron carbide produces small, shallow crater topography on Ti_6Al_4V but results in high dielectric fluid consumption during machining [69]. Neglecting these interaction effects can lead to an incomplete or even misleading interpretation of the process mechanics and hinder precise control of the surface finish. Thus, while the individual contributions of PonT and OV to CW are clearly substantial, a thorough analysis that incorporates their interaction would provide invaluable insights into optimising the WEDM process to achieve the desired surface characteristics in heat-treated high-carbon alloy steel. The residual plot for CW response is shown in Figure 10. The data in this research are normally distributed, as indicated by most of the blue dots clustering near the red line in the normal probability plot. Versus fits and Versus order display residuals scattered randomly around zero with no apparent pattern. These diagnostics collectively imply that the regression model assumptions are reasonably met.

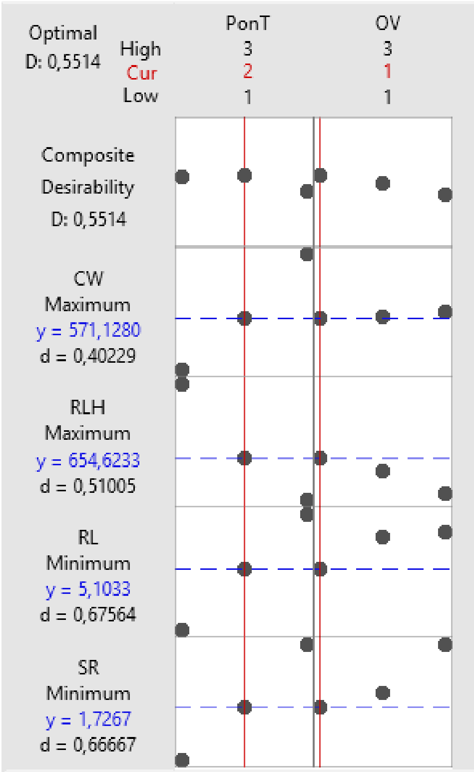

Figure 11. Results of ANOVA response optimiser

3.5 ANOVA Response Optimisation

The steps of the ANOVA response optimiser are performed after a thorough examination of microscopic defects, including SR, RL, RLH, and CW. The response determination is selected as the minimum SR, the minimum RL thickness, the maximum RLH, and the maximum CW. Figure 11 displays the multi-objective response optimisation of the WEDM process, designed to determine the optimal combination of PonT and OV that balances surface integrity characteristics. The objective of the optimisation process was to maximise RLH and CW, while simultaneously minimising RL thickness and SR. The subsequent optimisation analysis identified an optimal parameter set with PonT = 0.4 µs (Level 2) and OV = 90 V (Level 1). The composite desirability for this optimal solution is 0.5514, indicating a moderate overall compromise among the potentially conflicting objectives. This outcome provides important insight into the practical application of the ANOVA results previously discussed. ANOVA revealed the significant main effects of both PonT and OV. The optimisation process was to maximise CW (desirability d = 0.40229). Its individual desirability is lower than that for minimising RL (d = 0.67564) and SR (d = 0.66667), and for maximising RLH (d = 0.51005). This suggests that achieving an exceptionally large CW might be at odds with simultaneously obtaining a smoother surface, a thinner RL, and harder RL properties, which are often prioritised for enhanced component performance. The optimal settings of PonT at 0.4 µs and OV at 90 V represent a strategic compromise, with intermediate PonT and lower OV values selected to balance PonT's strong influence across all responses. The objective of achieving a refined surface and a robust RL is thus realised. This demonstrates that quantitative understanding of individual parameter contributions derived from ANOVA can be translated into practical multi-objective process control for WEDM of hardened high-carbon steel. These optimisation results are excellent and represent the best optimal solution because they have the highest multi-response compromise value. Other research achieved a good predictive R^2 = 0.9646 using an artificial neural network approach for different dielectric fluids in WEDM [70].

4. Conclusion

This work systematically studied the microstructural characteristics of WEDM in hardened high-carbon steel and revealed important insights into how machining parameters influence surface integrity. The research proved the significant impact of PonT and OV on SR, RL thickness, RLH and CW. One of the important conclusions is that PonT is always more important than OV for all tested reactions. PonT and OV vary directly with SR, RL and CW. More aggressive material removal, larger craters, and thicker RLs can be obtained by increasing the energy per discharge, which can be achieved by increasing pulse durations or voltages. However, these factors were negatively associated with RLH. The increased energy input accelerates melting and ejection of materials, but also decreases the cooling rates within the molten pool. This results in a more flexible and less dense RL due to changes in the microstructure. The relation of these responses is clear. Deep craters are formed, and the RL is thick and irregular. This makes the surface rougher and the RL more flexible. From a practical perspective, these results are highly useful for improving WEDM processes in industries that deal with high-carbon steels and have stringent requirements for surface quality and mechanical performance. To limit unwanted surface imperfections, such as high SR, high RL and large craters, manufacturers should aim for lower PonT and OV settings, and work to achieve a more robust RL.

This proposed parameter window mitigates harsh heat effects, resulting in improved surface polish and a robust RL. The PonT parameter settings were altered to obtain low SR, RL thickness, and CW results, and high LRH results for the heat-treated Buderus 2080 material. The results showing that RLs of untreated materials were larger and more irregular suggest that material pretreatment and accurate control of WEDM parameters are both important to achieve the desired surface integrity. The ANOVA response optimiser was used to optimise RLH and CW maximising, while RL thickness and SR were minimised. The optimisation analysis showed an optimal set of parameters with PonT = 0.4 µs and OV = 90 V. The macro performance of WEDM across different environments could be analysed in future work to improve this study and investigate additional output characteristics beyond microscopic surface integrity. Furthermore, the importance of these findings could be enhanced by exploring the WEDM responses of different material types. The following research should investigate the influence of other parameters, such as PofT duration and wire feed, which are known to affect energy dissipation and debris removal, on the surface topography and the properties of the RL.

Acknowledgements
The authors would like to express their profound gratitude and appreciation to the International Collaboration Programme of Lembaga Penelitian dan Pengabdian Masyarakat (Institute for Research and Community Service) at Universitas Trunojoyo Madura for the invaluable support that ensured the success of this project.

Funding
This study was not supported by any grants from funding bodies in the public, private, or not-for-profit sectors.

Declaration of Competing Interest
The authors declare that there are no known competing financial interests or personal relationships that could have influenced the work reported in this paper.

CRediT Authorship Contribution Statement
Rifky Maulana Yusron: Conceptualisation; Methodology; Analysis; Writing - draft & review; Supervision, Validation
Yuli Panca Asmara: Conceptualisation; Formal analysis; Writing - Draft; Supervision
Ananto Yusuf Wicaksono: Formal analysis; Investigation; Conceptualisation; Visualisation; Writing – revise &
Muhammad Azmi Alamsyah: Methodology; Data curation; Resources, Writing – revise & review

Availability of Data and Materials
The datasets generated and/or analysed during the current study are available from the corresponding author on reasonable request.

Ethics Statement
This study did not involve human participants or animal subjects. Ethical approval was therefore not required for this research.

Generative Artificial Intelligence Declarations
The authors claim that artificially intelligent-assisted technologies, such as generative AI, were not used to generate content, ideas, or theories. We have just utilised AI to enhance readability and refine the language. This was used with extreme human control and oversight. The authors take full responsibility for reviewing and approving the content.

References

[1] M. N. Alam, A. N. Siddiquee, Z. A. Khan, and N. Z. Khan, "A comprehensive review on wire EDM performance evaluation," *Proceedings of the Institution of Mechanical Engineers, Part E: Journal of Process Mechanical Engineering*, 2022, vol. 236, no. 4, pp. 1724–1746. https://doi.org/10.1177/09544089221074843

[2] T. Van Riel, J. Qian, and B. Lauwers, "Wire EDM roughing and Wire ECM finishing of 316L stainless steel on a single platform–An investigation of the combined strategy on surface quality and precision," *CIRP Annals*, vol. 73, no. 1, pp. 109–112, 2024. https://doi.org/10.1016/j.cirp.2024.04.042

[3] Ľ. Straka, and I. Čorný, "Prediction and multiparametric optimization of the machined surface quality of tool steels in precise wire electrical discharge machining," *Machines*, vol. 12, no. 4, p. 248, 2024, https://doi.org/10.3390/machines12040248
[4] A. S. S. Balan, and A. Giridharan, "A progress review in wire electrical discharge machining process," *International Journal of Automotive and Mechanical Engineering*, vol. 14, no. 2, pp. 4097–4124, 2017. https://doi.org/10.15282/ijame.14.2.2017.1.0330.
[5] A. W. Kebede, P. Promod Kumar, and C. K. Sahoo, "Machining efficiency and geometrical accuracy on micro-EDM drilling of titanium alloy," *Materials and Manufacturing Processes*, vol. 39, no. 10, pp. 1380–1395, 2024. https://doi.org/10.1080/10426914.2024.2323438
[6] S. Pawanr, and K. Gupta, "A review on recent advances in the energy efficiency of machining processes for sustainability," *Energies*, vol. 17, no. 15, p. 3659, 2024. https://doi.org/10.3390/en17153659
[7] J. V. Abellán-Nebot, C. Vila Pastor, and H. R. Siller, "A review of the factors influencing surface roughness in machining and their impact on sustainability," *Sustainability*, vol. 16, no. 5, p. 1917, 2024. https://doi.org/10.3390/su16051917
[8] L. A. Sosnovskii, V. V Komissarov, and S. S. Shcherbakov, "A method of experimental study of friction in a active system," *Journal of Friction and Wear*, vol. 33, no. 2, pp. 136–145, 2012. https://doi.org/10.3103/S1068366612020110
[9] K. Stevens, "Characterisation and quality control of surface treatments and coatings," in *Surface Engineering*, S.A. Meguid, Ed., Dordrecht: Springer Netherlands, 1990, pp. 1–13. https://doi.org/10.1007/978-94-009-0773-7_1
[10] A. Goyal, A. Garimella, and P. Saini, "Optimisation of surface roughness by design of experiment techniques during wire EDM machining," *Material Today: Proceeding*, 2021, vol. 47, pp. 3195–3197. https://doi.org/https://doi.org/10.1016/j.matpr.2021.06.302
[11] I. Aswith Babu, S. Kumar Manjhi, P. Sekar, and A. S. S. Balan, "Effect of Wire-EDM textures on corrosion performance of Bio-Degradable Mg alloy," *Material Letters*, vol. 372, p. 137088, 2024. https://doi.org/https://doi.org/10.1016/j.matlet.2024.137088
[12] A. Subburaj, V.A. Chandramoorthy, and S. Chinnaraj, "Parameter optimisation of wire-cut EDM on inconel alloy for maximizing material removal rate," *Engineering Proceedings*, vol. 61, no. 1, p. 34, 2024, https://doi.org/10.3390/engproc2024061034
[13] V. Krishnan, S. Sampath, A. Anbalagan, V. Paneerselvam, and V. Karthick, "Wire EDM process of AISI 431 martensitic stainless steel: A machinability investigation," *Engineering Proceedings*, 2024, vol. 61, no. 27, pp. 1–4. https://doi.org/10.3390/engproc
[14] M. Wasif, Y. Ahmed Khan, A. Zulqarnain, and S. Amir Iqbal, "Analysis and optimisation of wire Electro-Discharge Machining process parameters for the efficient cutting of Aluminum 5454 alloy," *Alexandria Engineering Journal*, vol. 61, no. 8, pp. 6191–6203, 2022. https://doi.org/10.1016/j.aej.2021.11.048
[15] M. A. Singh, K. Joshi, O. Hanzel, R. Singh, P. Sajgalik, and D. Marla, "Influence of open voltage and servo voltage during Wire-EDM of silicon carbides," in *Procedia CIRP*, Elsevier B.V., 2020, pp. 285–289. https://doi.org/10.1016/j.procir.2020.02.305
[16] D. Pendokhare, and S. Chakraborty, "A review on multi-objective optimisation techniques of wire electrical discharge machining," *Archives of Computational Methods in Engineering*, vol. 32, no. 3, pp. 1797–1839, 2025. https://doi.org/10.1007/s11831-024-10195-3
[17] S. Kumar, and M. Bohat, A. Info, "Effects of process parameters on MRR and surface roughness during WEDM of 309H stainless steel," *International Journal for Modern Trends in Science and Technology*, vol. 7, no. 12, pp. 54–67, 2021. https://doi.org/10.46501/IJMTST0712010
[18] B. Nosek, and T. Errington, "What is replication?" *PLoS Biology*, vol. 18, p. e3000691, 2020. https://doi.org/10.1371/journal.pbio.3000691
[19] K. L. Fowler, and M. D. Fleming, "Chapter 58 - Principles and methods of randomisation in research," in *Translational Surgery*, A.E.M. Eltorai, J.A. Bakal, P.C. Newell, A.J. Osband, Eds., Academic Press, 2023, pp. 353–358. https://doi.org/10.1016/B978-0-323-90300-4.00038-0
[20] J. Wittenburg, U. Küpper, T. Herrig, A. Klink, and T. Bergs, "Surface integrity analysis of single discharge characteristics derived from the continuous wire EDM process," in *Procedia CIRP*, Elsevier B.V., 2024, pp. 203–208. https://doi.org/10.1016/j.procir.2024.05.037
[21] C. Yang, Y. Li, S. Han et al., "Effects of solid–solution temperature on microstructures and mechanical properties of 2200 MPa grade secondary hardening steel," *Materials*, vol. 18, no. 9, p. 2126, 2025. https://doi.org/10.3390/ma18092126.
[22] Z. Lian, J. Zhou, W. Ren et al., "Recent progress in bio-inspired macrostructure array materials with special wettability—from surface engineering to functional applications," *International Journal of Extreme Manufacturing*, vol. 6, no. 1, p. 012008, 2024. https://doi.org/10.1088/2631-7990/ad0471
[23] A. Goyal, A. Pandey, and H. U. R. Rahman, "Present and future prospective of shape memory alloys during machining by EDM/wire EDM process: A review," *Sādhanā*, vol. 47, no. 4, p. 217, 2022. https://doi.org/10.1007/s12046-022-01999-9
[24] S. K. Chaubey, and K. Gupta, "An experimental study on out-of-roundness and material erosion rate during wire spark erosion turning of titanium cylindrical bars," *Journal of Materials Research and Technology*, vol. 24, pp. 7539–7551, 2023. https://doi.org/10.1016/j.jmrt.2023.05.027

[25] S. S. Patel, and D. M. Patel, "Investigation of machining characteristics of SKD 11 in WEDM," *Material Today: Proceeding*, 2022, vol. 59, pp. 468–475. https://doi.org/10.1016/j.matpr.2021.11.468
[26] S. Ezeddini, M. Boujelbene, E. Bayraktar, and S. Ben Salem, "Optimisation of the surface roughness parameters of Ti–Al intermetallic based composite machined by wire electrical discharge machining," *Coatings*, vol. 10, no. 9, p. 900, 2020. https://doi.org/10.3390/coatings10090900
[27] R. Sen, S. Paul, and B. Choudhuri, "Investigation on wire electrical discharge machining of AISI 304 stainless steel," *Material Today: Proceeding*, 2022, vol. 62, pp. 1210–1214. https://doi.org/10.1016/j.matpr.2022.04.458
[28] J. Buk, "Surface topography of Inconel 718 alloy in finishing WEDM," *Advances in Science and Technology Research Journa*l, vol. 16, no. 1, pp. 47–61, 2022. https://doi.org/10.12913/22998624/142962
[29] D. Marelli, S. K. Singh, S. Nagari, and R. Subbiah, "Optimisation of machining parameters of wire-cut EDM on super alloy materials–A review," *Material Today: Proceeding*, vol. 26, pp. 1021-1027, 2020. doi: https://doi.org/10.1016/j.matpr.2020.01.306
[30] M. E. Asgar, and A. K. Singh Singholi, "Parameter study and optimisation of WEDM process: A Review," *IOP Conference Series: Materials Science and Engineering*, vol. 404, no. 1, p. 012007, 2018. https://doi.org/10.1088/1757-899X/404/1/012007
[31] C. Xu, F. Xu, F. Sun et al., "Research on an intelligent control method of a magnetic actuator for micro electrical discharge machining," *Actuators*, vol. 11, no. 12, p. 371, 2022. https://doi.org/10.3390/act11120371
[32] U. Küpper, T. Herrig, D. Welling, and T. Bergs, "Process performance of high energy wire EDM," in *Procedia CIRP*, Elsevier B.V., 2020, pp. 230–233. https://doi.org/10.1016/j.procir.2020.11.012
[33] L. Selvarajan, R. Rajavel, K. Venkataramanan, and V. P. Srinivasan, "Experimental investigation on surface morphology and recasting layer of Si3N4-TiN composites machined by die-sinking and rotary EDM," *Ceramics International*, vol. 49, no. 5, pp. 8487–8501, 2023. https://doi.org/10.1016/j.ceramint.2022.11.011
[34] S. Ezeddini, W. Rajhi, M. Boujelbene, E. Bayraktar, and S. Ben Salem, "An investigation to achieve good surface integrity in wire electrical discharge machining of Ti-6242 super alloy," *Journal of Materials Engineering and Performance*, vol. 33, no. 9, pp. 4523–4537, 2024. https://doi.org/10.1007/s11665-023-08270-0
[35] S. Chakraborty, H. N. Datta, and S. Chakraborty, "Grey relational analysis-based optimization of machining processes: A comprehensive review," *Process Integration and Optimization for Sustainability*, vol. 7, no. 4, pp. 609–639, 2023. https://doi.org/10.1007/s41660-023-00311-4
[36] A. A. Azawqari, M. A. Amrani, L. Hezam, M. Baggash, and Z. Z. Abidin, "Multi-objectives optimisation of WEDM parameters on machining of AISI 304 based on Taguchi method," *The International Journal of Advanced Manufacturing Technology*, vol. 134, no. 11, pp. 5493–5510, 2024. https://doi.org/10.1007/s00170-024-14423-9
[37] B. K. Kumar, and V. C. Das, "Perspective and prospects of wire electric discharge machining (WEDM)," *Journal of Engineering and Technological Sciences*, vol. 54, no. 5, 2022. https://doi.org/10.5614/j.eng.technol.sci.2022.54.5.9
[38] J. K. Abbas, S. H. Aghdeab, and A. Al-Habaibeh, "Investigating the effect of process parameters on surface roughness of AISI M2 steel in EDM using deep learning neural networks," *International Journal of Advanced Manufacturing Technology*, vol. 137, no. 1, pp. 251–262, 2025. https://doi.org/10.1007/s00170-025-15184-9
[39] I. Ayesta, B. Izquierdo, O. Flaño, J.A. Sánchez, J. Albizuri, R. Avilés, "Influence of the WEDM process on the fatigue behavior of Inconel® 718," *International Journal of Fatigue*, vol. 92, pp. 220–233, 2016. https://doi.org/10.1016/j.ijfatigue.2016.07.011
[40] K. Hareesh, K. V Nalina Pramod, N. K. Linu Husain, K. B. Binoy, R. D. Kumar, and N. K. Sreejith, "Influence of process parameters of wire EDM on surface finish of Ti6Al4V," *Material Today: Proceeding*, 2021, vol. 47, pp. 5017–5023. https://doi.org/10.1016/j.matpr.2021.04.590
[41] J. E. A. Qudeiri, A. Zaiout, A. H. I. Mourad, and M. H. Abidi, A. Elkaseer, "Principles and characteristics of different EDM processes in machining tool and die steels," *Applied Sciences (Switzerland)*, vol. 10, no. 6, p. 2082, 2020. https://doi.org/10.3390/app10062082
[42] W. Ming, Z. Xie, J. Ma et al., "Critical review on sustainable techniques in electrical discharge machining," *Journal of Manufacturing Processes*, vol. 72, pp. 375–399, 2021. https://doi.org/10.1016/j.jmapro.2021.10.035
[43] S. Chakraborty, S. Mitra, and D. Bose, "An investigation on dimensional accuracy and surface topography in powder mixed WEDM using RSM and GRA-PCA," *Material Today: Proceeding*, 2021, vol. 44, pp. 1524–1530. https://doi.org/10.1016/j.matpr.2020.11.734
[44] D. Doreswamy, D. Sai Shreyas, S. K. Bhat, and R. N. Rao, "Optimisation of material removal rate and surface characterisation of wire electric discharge machined Ti-6Al-4V alloy by response surface method," *Manufacturing Review (Les Ulis)*, vol. 9, p. 15, 2022. https://doi.org/10.1051/mfreview/2022016
[45] H. Singh, J. Singh, and S. Kumar, "Effect of processing conditions and electrode materials on the surface roughness of EDM-processed hybrid metal matrix composites," *International Journal of Lightweight Materials and Manufacture*, vol. 7, no. 3, pp. 480–493, 2024. https://doi.org/10.1016/j.ijlmm.2023.12.001
[46] C. Sarala Rubi, J. U. Prakash, S. J. Juliyana et al., "Comprehensive review on wire electrical discharge machining: A non-traditional material removal process," *Frontiers in Mechanical Engineering*, vol. 10, p. 1322605, 2024. https://doi.org/10.3389/fmech.2024.1322605
[47] K. Paswan, S. Sharma, S. P. Dwivedi et al., "An analysis of microstructural morphology, surface topography, surface integrity, recast layer, and machining performance of graphene nanosheets on Inconel 718 superalloy: Investigating

the impact on EDM characteristics, surface characterisations, and optimisation," *Journal of Materials Research and Technology*, vol. 27, pp. 7138–7158, 2023. https://doi.org/10.1016/j.jmrt.2023.11.080

[48] W. Rajhi, I. Alatawi, T. Subhani, B. Ayadi, A. Al-Ghamdi, and A. Khaliq, "A contribution to numerical prediction of surface damage and residual stresses on die-sinking EDM of Ti6Al4V," *Journal of Manufacturing Processes*, vol. 68, pp. 1458–1484, 2021. https://doi.org/10.1016/j.jmapro.2021.06.056

[49] M. F. Mohamed, and K. Lenin, "Optimisation of wire EDM process parameters using Taguchi technique," *Material Today: Proceeding*, 2020, vol. 21, pp. 527–530. https://doi.org/10.1016/j.matpr.2019.06.662

[50] P. M. Abhilash, D. Chakradhar, "Surface integrity comparison of wire electric discharge machined Inconel 718 surfaces at different machining stabilities," in *Procedia CIRP*, Elsevier B.V., 2020, pp. 228–233. https://doi.org/10.1016/j.procir.2020.02.037

[51] M. J. Madu, O. Adedipe, S. A. Lawal, and A. S. Abdulrahman, "The influence of carburisation parameters on the mechanical behavior of mild steel: A review," *Journal of Engineering and Applied Science*, vol. 72, no. 1, p. 193, 2025, Springer Nature. https://doi.org/10.1186/s44147-025-00776-9

[52] H. Boumediri, S. Touati, Y. Debbah et al., "Effect of carburising time treatment on microstructure and mechanical properties of low alloy gear steels," *Materials Research Express*, vol. 11, no. 7, p. 076505, 2024. https://doi.org/10.1088/2053-1591/ad5cd6

[53] B. Gugulothu, R. D. Ramachandran, K. Kumar et al., "Investigation of surface morphology and surface roughness of AISI 304 stainless steel in WEDM: Experimental optimization and prediction using machine learning," *Journal of Materials Research and Technology*, vol. 41, pp. 6251–6263, 2026. https://doi.org/10.1016/j.jmrt.2026.02.151

[54] J. Gao, H. Lan, Q. Jiang et al., "Mechanisms of hardness variation in 14Cr12Ni3Mo2VN martensitic stainless steel under different tempering temperatures following high-frequency induction quenching," *Coatings*, vol. 15, no. 3, p. 306, 2025. https://doi.org/10.3390/coatings15030306

[55] T. Loaiza, R. P. Babu, S. Ooi, and P. Hedström, "Refining the mechanistic understanding of microstructural decay during rolling contact fatigue in 52100 bearing steel tempered at high temperature," Journal of Materials Science, vol. 58, no. 44, pp. 17093–17112, 2023. https://doi.org/10.1007/s10853-023-09088-w

[56] M. Rao, V. Vijayan, A. Anil, P. K. Rai, and N. R. Jain, "Effect of wire electrode discharge machining process parameters on the surface roughness, hardness, and microstructure of the high carbon steels," *Material Today: Proceeding*, 2021, vol. 46, pp. 2625–2629. https://doi.org/10.1016/j.matpr.2021.02.269

[57] L. W. Reolon, C. A. Henning Laurindo, R. D. Torres, and F. L. Amorim, "WEDM performance and surface integrity of Inconel alloy IN718 with coated and uncoated wires," *The International Journal of Advanced Manufacturing Technology*, vol. 100, no. 5, pp. 1981–1991, 2019. 10.1007/s00170-018-2828-6

[58] X. Chen, J. Sun, K. Li et al., "Effect of carburizing composite laser-shock processing on properties and microstructure of 20CrNiMo steel," *Metals (Basel)*, vol. 14, no. 1, p. 10, 2024. 10.3390/met14010010

[59] O. Gokcekaya, A. Günen, F. Ceritbinmez, A. Bahador, T. Nakano, and M. Çetin, "Wire-EDM performance and surface integrity of Inconel 718 with unique microstructural features fabricated by laser powder bed fusion," *The International Journal of Advanced Manufacturing Technology*, vol. 130, no. 9, pp. 4513–4528, 2024. https://doi.org/10.1007/s00170-023-12924-7

[60] F. Yu, Y. Zhang, C. Kong, and H. Yu, "Microstructure and mechanical properties of Ti–6Al–4V alloy sheets via room-temperature rolling and cryorolling," *Materials Science and Engineering: A*, vol. 834, p. 142600, 2022. https://doi.org/10.1016/j.msea.2022.142600

[61] R. Sen, S. Paul, and B. choudhuri, "Investigation on wire electrical discharge machining of AISI 304 stainless steel," *Material Today: Proceeding*, 2022, vol. 62, pp. 1210–1214. https://doi.org/10.1016/j.matpr.2022.04.458

[62] S. Jayakumar, L. Jayakumar, and U. Elaiyarasan, "An investigation on surface integrity and microstructure behaviour of AISI 304 stainless steel machined by die sinking EDM," *Metallurgical Research & Technology*, vol. 121, no. 5, p. 511, 2024. https://doi.org/10.1051/metal/2024065

[63] J. Yan, C. Zhang, J. Guo et al., "Investigating the influence mechanisms of cryogenic treatment on mechanical properties and wear resistance of AISI 4340 steel," *Journal of Materials Research and Technology*, vol. 38, pp. 3264–3276, 2025. https://doi.org/10.1016/j.jmrt.2025.08.142

[64] A. Hedayati, A. Najafizadeh, A. Kermanpur, and F. Forouzan, "The effect of cold rolling regime on microstructure and mechanical properties of AISI 304L stainless steel," *Journal of Materials Processing Technology*, vol. 210, no. 8, pp. 1017–1022, 2010. https://doi.org/10.1016/j.jmatprotec.2010.02.010

[65] N. Jin, Z. Yan, Y. Wang, H. Cheng, and H. Zhang, "Effects of heat treatment on microstructure and mechanical properties of selective laser melted Ti-6Al-4V lattice materials," *International Journal of Mechanical Sciences*, vol. 190, p. 106042, 2021. https://doi.org/10.1016/j.ijmecsci.2020.106042

[66] V. Šimna, M. Kuruc, B. Ludrovcová, A. Belanec, V. Kolesnyk, and O. Berezniak, "Wire electrode wear in WEDM of Inconel 718: Gravimetric evaluation using a 33 full factorial design," *Applied Sciences*, vol. 16, no. 11, p. 5235, 2026. https://doi.org/10.3390/app16115235

[67] K. Natarajan, H. Ramakrishnan, A. Gacem et al., "Study on optimisation of WEDM process parameters on stainless steel," *Journal of Nanomaterial*, vol. 2022, no. 1, pp. 1–7, 2022. https://doi.org/10.1155/2022/6765721

[68] M. S. Tufail, J. Giri, E. Makki, T. Sathish, R. Chadge, and N. Sunheriya, "Machinability of different cutting tool materials for electric discharge machining: A review and future prospects," *American Institute of Physics Advance*, vol. 14, no. 4, pp. 1–28, 2024. https://doi.org/10.1063/5.0201614

[69] S. Chakraborty, S. Mitra, D. Bose, "Performance analysis on eco-friendly machining of Ti6Al4V using powder mixed with different dielectrics in WEDM," *International Journal of Automotive and Mechanical Engineering*, vol. 17, no. 3, pp. 8128–8139, 2020. https://doi.org/10.15282/IJAME.17.3.2020.06.0610

[70] D. Sakthimurugan, K. Thavasilingam, A. P. Murali, A. P. Kumar, P. Vijayakumar, and M. D. Barath Kumar, "Optimization of AA7075-SiC Composite Machining by WEDM Using Biosilica Additives," *International Journal of Automotive and Mechanical Engineering*, vol. 22, no. 4, pp. 1–19, 2025. https://doi.org/10.15282/ijame.22.4.2025.18.0995